

RESEARCH ARTICLE

A Chimera Na⁺-Pump Rhodopsin as an Effective Optogenetic Silencer

Mohammad Razuanul Hoque¹, Toru Ishizuka¹, Keiichi Inoue^{2,3,4,5}, Rei Abe-Yoshizumi², Hiroyuki Igarashi^{6,7}, Takaaki Mishima¹, Hideki Kandori^{2,3}, Hiromu Yawo^{1,6*}

1 Department of Developmental Biology and Neuroscience, Tohoku University Graduate School of Life Sciences, Sendai, 980–8577, Japan, **2** Department of Life Science and Applied Chemistry, Nagoya Institute of Technology, Showa-ku, Nagoya, 466–8555, Japan, **3** OptoBioTechnology Research Center, Nagoya Institute of Technology, Showa-ku, Nagoya, 466–8555, Japan, **4** PRESTO, Japan Science and Technology Agency, 4-1-8 Honcho, Kawaguchi, Saitama, 332–0012, Japan, **5** Frontier Research Institute for Material Science, Nagoya Institute of Technology, Showa-ku, Nagoya, 466–8555, Japan, **6** Department of Physiology and Pharmacology, Center for Neuroscience, Tohoku University Graduate School of Medicine, Sendai, 980–8577, Japan, **7** Tohoku University Division For Interdisciplinary Advanced Research and Education, Sendai, 980–8578, Japan

* hiromu.yawo.c7@tohoku.ac.jp



OPEN ACCESS

Citation: Hoque MR, Ishizuka T, Inoue K, Abe-Yoshizumi R, Igarashi H, Mishima T, et al. (2016) A Chimera Na⁺-Pump Rhodopsin as an Effective Optogenetic Silencer. PLoS ONE 11(11): e0166820. doi:10.1371/journal.pone.0166820

Editor: Steven Barnes, Dalhousie University, CANADA

Received: July 13, 2016

Accepted: November 5, 2016

Published: November 18, 2016

Copyright: © 2016 Hoque et al. This is an open access article distributed under the terms of the [Creative Commons Attribution License](https://creativecommons.org/licenses/by/4.0/), which permits unrestricted use, distribution, and reproduction in any medium, provided the original author and source are credited.

Data Availability Statement: All relevant data are within the paper and its Supporting Information files.

Funding: This study was supported by a Grant-in-Aid for Scientific Research (No. 25250001 to HY and No. 25290002 to TI) from the Ministry of Education, Culture, Sports, Science and Technology (MEXT) of Japan: <http://www.jpsps.go.jp/english/e-grants/grants01.html>, a Grant-in-Aid for Scientific Research on Innovative Areas “Adaptive Circuit Shift” (No. 15H01413 to HY) of the Ministry of Education, Culture, Sports, Science and Technology (MEXT) of Japan: <http://www.jpsps>.

Abstract

With the progress of optogenetics, the activities of genetically identified neurons can be optically silenced to determine whether the neurons in question are necessary for the network performance of the behavioral expression. This logical induction is expected to be improved by the application of the Na⁺ pump rhodopsins (NaRs), which hyperpolarize the membrane potential with negligible influence on the ionic/pH balance. Here, we made several chimeric NaRs between two NaRs, KR2 and *Ia*NaR from *Krokinobacter eikastus* and *Indibacter alkaliphilus*, respectively. We found that one of these chimeras, named *I₁K₆NaR*, exhibited some improvements in the membrane targeting and photocurrent properties over native NaRs. The *I₁K₆NaR*-expressing cortical neurons were stably silenced by green light irradiation for a certain long duration. With its rapid kinetics and voltage dependency, the photoactivation of *I₁K₆NaR* would specifically counteract the generation of action potentials with less hyperpolarization of the neuronal membrane potential than KR2.

Introduction

A neural system is a kind of computing system comprised by a vast number of neurons. Understanding of the significance of a neuron or a set of neurons in a network has been one of the major goals of neuroscience. In recent years the optical methods have been developed to manipulate genetically targeted neurons using light under precise spatiotemporal resolution [1–4]. For example, the neuronal excitability is enhanced by light if light-sensitive cation channels such as channelrhodopsin-2 (ChR2) are expressed in a neuron [5,6]. The resulting neural network or behavior responses suggest that the stimulated neuron is involved in the responses as a sufficient condition, although it is necessary to avoid oversimplification [4]. On the other hand, optical silencing of the neural activity could determine whether the neuron in question is necessary for the network performance of the behavioral expression.

go.jp/english/e-grants/grants01.html, a Grant-in-Aid for challenging Exploratory Research (No. 15K15025 to HY), MEXT, Japan: <http://www.jsps.go.jp/english/egrants/grants01.html> and JST, Strategic International Collaborative Research Program, SICORP.

Competing Interests: The authors have declared that no competing interests exist.

In the field of the optogenetics, the microbial Cl⁻-pump rhodopsins such as a halorhodopsin from *Natronomonas pharaonis* (NpHR) and the microbial H⁺-pump rhodopsins such as archaerhodopsins from *Halorubrum sodomense* (AR3/ArchT) are now the most widely used loss-of-function tools, which effectively hyperpolarize the membrane potential to inhibit the generation of action potentials [7–11]. Recently, Cl⁻/anion channel rhodopsins have become another potential candidates for the purpose of optogenetic silencing of the neural activities [12–15]. Although they have made great progress, these tools still have some disadvantages such as inevitable changes in the ionic/pH balance between the intracellular and extracellular milieu [1,16,17]. In addition, in the case of Cl⁻/anion channel rhodopsins, the direction of the membrane potential change should be dependent on the Cl⁻-equilibrium potential, which can be affected by many factors such as development, localization and disease [18–25]. On the other hand, a new microbial rhodopsin named KR2 from the marine flavobacterium *Krokinobacter eikastus*, was characterized as one of the light-driven Na⁺ pumps that transport Na⁺ from the inside to the outside of the expressed cell under physiological conditions [26]. As the natural excitatory signals generally induce Na⁺ influx through non-selective cation channels, the Na⁺ pump rhodopsins (NaRs) are ideal tools to reduce the neuronal excitability by light, but with minimal influence on the ionic/pH balance [27].

Recently the numbers of NaRs are increasing to form a large subfamily of microbial rhodopsins [28]. Here, we characterized one of the microbial rhodopsins named *IaNaR* from *Indibacter alkaliphilus* as a new NaR that transports Na⁺ from the inside to the outside of the expressed cell under physiological conditions. The ion-transporting activity of *IaNaR* was inefficient when exogenously expressed in mammalian cells. However, one of the chimeric NaRs between *IaNaR* and KR2 exhibited some improvements in the membrane targeting and photocurrent properties over native ones. It is anticipated that the chimeric NaRs will become useful to counteract the generation of action potentials when expressed in neurons as an optogenetic silencing tool.

Materials and Methods

Protein expression and purification

The synthesized *IaNaR* gene, whose codons were optimized for *E. coli* expression, was inserted into the Nde I-Xho I site of pET21a vector, with the resulting construct encoding a His₆ tag at the C-terminus. The expression plasmid of *IaNaR* was transformed in to *E. coli* C41(DE3) and the rhodopsins were overexpressed in the cells induced with 1 mM isopropyl-β-D-thiogalactopyranoside (IPTG) and 10 μM all-*trans* retinal for 4 hours. The crude membrane was solubilized with 1.5% n-dodecyl-β-D-maltoside (DDM), and the solubilized fraction was purified by TALON Metal Affinity Resin (Clontech Laboratories Inc., Mountain View, CA, USA).

Measurement of ion-transport activity

The *IaNaR* expressing cells were collected by centrifugation (4,800×g, 2 min), washed three times and resuspended in the same solvent (in mM), 100 NaCl, 100 Na₂SO₄ or 100 KCl, as for ion-transport measurement. The cell suspension was placed in the dark and then illuminated by using a 1-kW tungsten-halogen projector lamp (Master HILUX-HR, Rikagaku, Japan) through a glass filter (Y-52, AGC Techno Glass, Japan) for 2.5 min at wavelengths > 500 nm. The light-induced pH changes during incubation were monitored with a pH meter (F-55, Horiba, Japan).

Molecular biology

The CMV promoter-based expression plasmids encoding KR2, *IaNaR*, or its chimeras fused in-frame with a membrane trafficking signal (TS), an enhanced yellow fluorescent protein

(eYFP), and an ER export signal (ER_{ex}) were prepared as previously reported [27]. Both TS and ER_{ex} were derived from a Kir2.1 potassium channel with amino acid sequences of “N-KSRITSEGEYIPLDQIDINV-C (20 amino acids)” and “N-FCYENEV-COOH (7 amino acids)”, respectively [29]. The cDNAs encoding chimeras between *E. coli* codon-optimized *IaNaR* and human codon-optimized KR2 were prepared using In-Fusion cloning technology (Takara Bio, Shiga, Japan). Briefly, the amino acid sequences of the apoprotein were divided into seven transmembrane domains (TMDs) so that each TMD contained a transmembrane helix. These segments are referred to (from N-terminal to C-terminal) as “TMD1”, “TMD2”, “TMD3”, “TMD4”, “TMD5”, “TMD6”, and “TMD7” (Fig 1). The N-terminal transmembrane domains (TMDs) of KR2 were replaced in order with the homologous counterparts of *IaNaR* and thus we prepared 6 chimeras; *I*₁*K*₆NaR from TM1 (Met¹-Val⁵²) of *IaNaR* and TM2-7 (Asp⁵⁴-Ser²⁸⁰) of KR2, *I*₂*K*₅NaR from TM1-2 (Met¹-Asn¹⁰⁰) of *IaNaR* and TM3-7 (Asp¹⁰²-Ser²⁸⁰) of KR2, *I*₃*K*₄NaR from TM1-3 (Met¹-Val¹²⁷) of *IaNaR* and TM4-7 (Ser¹²⁹-Ser²⁸⁰) of

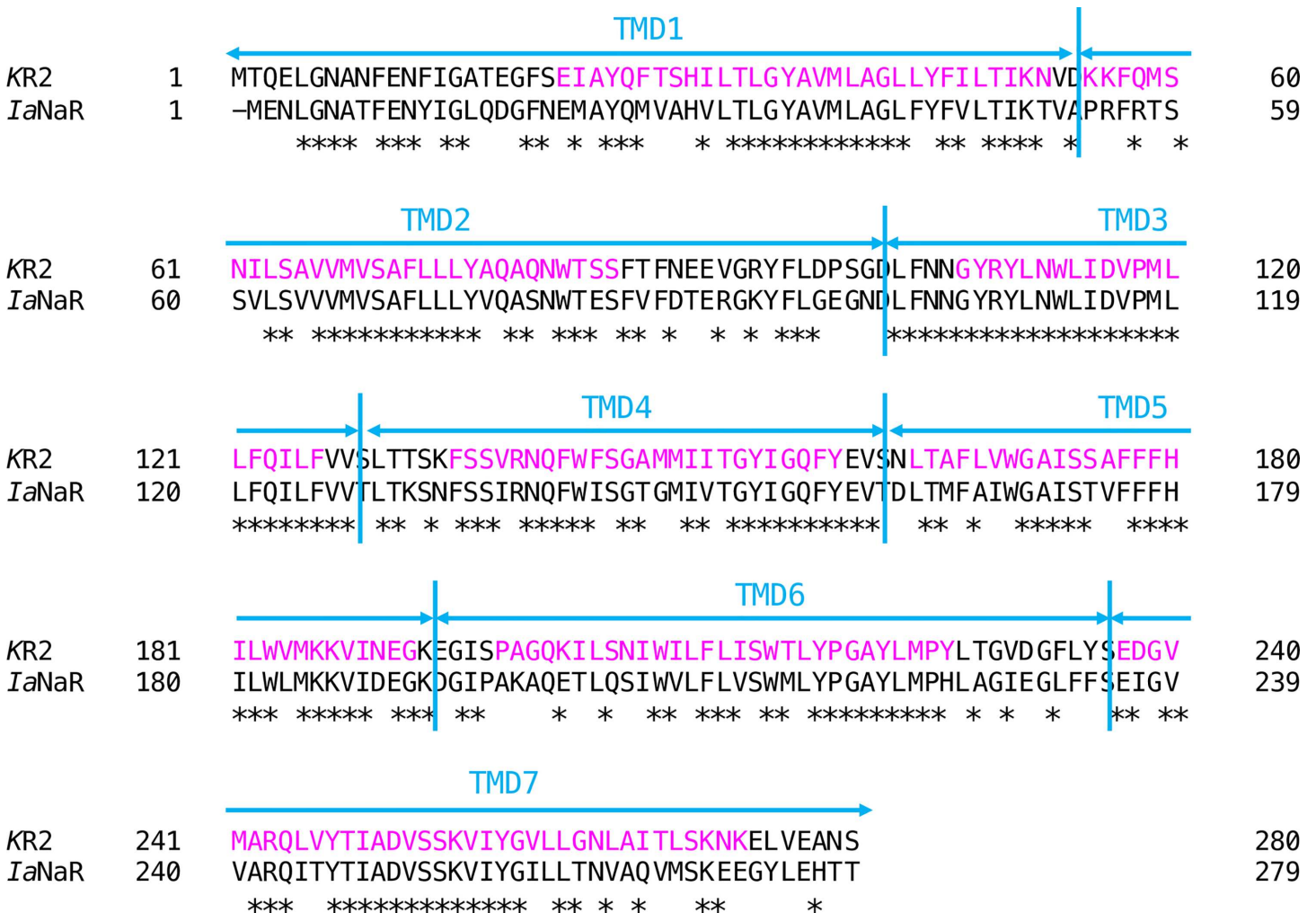


Fig 1. Primary structure of the Na⁺ pump rhodopsin (NaR) apoproteins. The sequence alignment of two NaRs, one from *Krokinobacter eikastus* (KR2, amino acids 1–280) and the other from *Indibacter alkaliphilus* (*IaNaR*, amino acids 1–279) is shown. Identical amino acids are indicated by an asterisk. The seven transmembrane helices of KR2 (Kato et al., 2015) are lettered in magenta. The amino acid sequences of the apoprotein were divided into seven transmembrane domains (TMDs) so that each TMD contain a transmembrane helix (cyan vertical lines). These segments are referred to (from the N-terminal to C-terminal) as “TMD1”, “TMD2”, “TMD3”, “TMD4”, “TMD5”, “TMD6”, and “TMD7”, respectively.

doi:10.1371/journal.pone.0166820.g001

KR2, I_4K_3 NaR from TM1-4 (Met¹-Val¹⁶⁰) of *Ia*NaR and TM5-7 (Ser¹⁶²-Ser²⁸⁰) of KR2, I_5K_2 NaR from TM1-5 (Met¹-Lys¹⁹²) of *Ia*NaR and TM6-7 (Glu¹⁹⁴-Ser²⁸⁰) of KR2 and I_6K_1 NaR from TM1-6 (Met¹-Phe²³⁴) of *Ia*NaR and TM7 (Ser²³⁶-Ser²⁸⁰) of KR2. For optimal expression in cultured neurons, the CMV enhancer/promoter was replaced with the CaMKII α promoter. All constructs were verified by sequencing.

All constructs were verified by sequencing, and submitted to DDBJ/EMBL/GenBank (<http://www.ddbj.nig.ac.jp/index-e.html>) with accession codes in the parentheses; human codon-optimized KR2 (Acc# LC012789), E. coli codon-optimized *Ia*NaR (Acc# LC187664), I_1K_6 NaR (Acc# LC187665), I_2K_5 NaR (Acc# LC187666), I_3K_4 NaR (Acc# LC187667), I_4K_3 NaR (Acc# LC187668), I_5K_2 NaR (Acc# LC187669) and I_6K_1 NaR (Acc# LC187670),

Mammalian cell culture

The electrophysiological assays of NaRs were made using ND7/23 cells as described previously [30]. Briefly, the cells were grown in Dulbecco's modified Eagle's medium (Wako, Osaka, Japan) supplemented with 2.5 μ M all-*trans* retinal, 10% fetal bovine serum under a 5% CO₂ atmosphere at 37°C. The expression plasmid encoding KR2, *Ia*NaR, or its chimeras was transiently transfected in ND7/23 cells using Effectene Transfection Reagent (Qiagen, Tokyo, Japan) according to the manufacturer's instructions. Electrophysiological recordings were then conducted 20–48 h after the transfection. Successfully transfected cells were identified by the presence of eYFP fluorescence.

Under anesthesia with a mixture (1 ml/kgBW) of ketamine (50 mg/ml, Daiichi Sankyo Co. Ltd., Tokyo, Japan) and xylazine (xylazine hydrochloride, 10 mg/ml, Sigma-Aldrich, St. Louis, MO, USA), the cortical neurons were isolated from embryonic day 16 Wistar rats (Japan SLC Inc., Shizuoka, Japan), using Nerve-Cells Dispersion Solutions (Wako) according to the manufacturer's instructions, and were grown in neuronal culture medium (Wako) under a 5% CO₂ atmosphere at 37°C. The neuronal expression plasmids were transiently transfected into cortical neurons by calcium phosphate transfection at days *in vitro* (DIV) 5 or 6. Electrophysiological recordings were then conducted at DIV 22–25 with neurons identified as expressing eYFP fluorescence by a conventional epifluorescence system.

All animal experiments were approved by the Tohoku University Committee for Animal Experiments (Approval No. 2014LSA-001) and were carried out in accordance with the Guidelines for Animal Experiments and Related Activities of Tohoku University as well as the guiding principles of the Physiological Society of Japan and the National Institutes of Health (NIH), USA. The number of animals in this study was kept to a minimum and, when possible, all animals were ketamine- xylazine anesthetized to minimize suffering.

Electrophysiology

All experiments were carried out at room temperature (23 \pm 2°C). Photocurrents were recorded as previously described [30] using an EPC-8 amplifier (HEKA Electronic, Lambrecht, Germany) under a whole-cell patch clamp configuration. The data were filtered at 1 kHz and sampled at 10 kHz (Digidata1440 A/D, Molecular Devices Co., Sunnyvale, CA) and stored in a computer (pClamp10.3, Molecular Devices). The photocurrent peak and steady-state (at the end of a 1-s light pulse) amplitudes were expressed as effective values (I_p and I_{ss} , respectively) after being divided by the whole-cell capacitance, which is proportional to the cell's surface area. For evaluating the magnitude of inactivation, the difference between I_p and I_{ss} was divided by I_p .

The internal pipette solutions for the whole-cell voltage clamp recordings from the ND7/23 cells contained (in mM): 20 NaOH, 100 L-glutamic acid Na salt, 5 EGTA, 50 HEPES, 2.5

MgCl₂, 2.5 MgATP, 0.1 leupeptin and pH 7.3 (adjusted by HCl). The cells were continuously superfused at a rate of 2 mL/min by ACSF solution (in mM): 125 NaCl, 2.5 KCl, 25 NaHCO₃, 1.25 NaH₂PO₄, 2 CaCl₂, 1 MgCl₂, 11 glucose, pH 7.4 and equilibrated with 95% O₂ and 5% CO₂.

The internal pipette solution for the whole-cell current-clamp recordings from cortical neurons contained (in mM): 125 K-gluconate, 10 NaCl, 0.2 EGTA, 10 HEPES, 1 MgCl₂, 3 MgATP, 0.3 Na₂GTP, 10 Na₂-phosphocreatine, 0.1 leupeptin and pH 7.4 adjusted with KOH. The cells were continuously superfused at a rate of 2 mL/min by ACSF solution equilibrated with 95% O₂ and 5% CO₂. In all cortical neuron experiments, the ACSF contained 100 μM picrotoxin (Nacalai Tesque, Kyoto, Japan) and 1 mM kynurenic acid (Sigma-Aldrich Co. LLC, St Louis, MS., USA) to block all synaptic inputs. The directly measured liquid junction potential was 11.4 mV and was compensated for.

Optics

Irradiation was performed using a SpectraX light engine (wavelength > 90% of the maximum, 534–600 nm, Lumencor Inc., Beaverton, Oregon, USA) controlled by computer software (pCLAMP10.3, Molecular Devices). The power density (irradiance) of the light was directly measured under microscopy by a visible light-sensing thermopile (MIR-101Q, SSC Co., Ltd., Kuwana City, Japan) and was 99 mW/mm². To investigate the action spectrum, irradiation was made at wavelengths (nm, >90% of the maximum, irradiance): 390 ± 18 (3.4 mW/mm²), 438 ± 24 (3.0 mW/mm²), 475 ± 28 (2.7 mW/mm²), 513 ± 17 (2.7 mW/mm²), 549 ± 15 (2.6 mW/mm²), 575 ± 25 (2.8 mW/mm²) and 632 ± 22 (2.8 mW/mm²).

Cytochemistry

Live cultured cells were reacted with 2 μg/ml of wheat germ agglutinin (WGA) conjugated with Alexa Fluor 633 (W21404, Thermo Fisher Scientific, Waltham, MA, USA) for 10 min at 37°C, then fixed with 4% paraformaldehyde. Localization was assessed by confocal microscopy (LSM710, Carl Zeiss, Oberkochen, Germany) equipped with ×63 oil objective lens. For the detection of each fluorescence substrate, the following optical combinations were used: a 488 nm argon laser and 523–620 nm bandpass filter for eYFP, a 633 nm HeNe laser and 638–747 nm bandpass filter for WGA.

For images of primary cultured cortical neurons, each pixel value of the relative fluorescent intensity was profiled along horizontal/vertical axes, which were delineated to pass the centroid of the cell (Zen software, Carl Zeiss), and the cross-correlation analysis between eYFP fluorescence and WGA fluorescence (Alexa Fluor 633) was performed for the pixel values between two points that were outside of the membrane to reach half of the peak amplitude of the WGA fluorescence (Clampfit 10, Molecular Devices). The overlapping index of a cell was defined as the average of 14 cross-correlation coefficients calculated for each lag of 0, ±1, ±2 and ±3 (the maximal distance, ±0.4 μm) along the horizontal and vertical axes. It was expected to be +1.0 when both profiles between eYFP and WGA are completely overlapped and to be -1.0 when there was no overlap.

Statistical analysis

All data in the text, figures and tables are expressed as mean ± SEM and were evaluated with the Mann-Whitney *U*-test for statistical significance unless otherwise noted. It was judged as statistically insignificant when *P* > 0.05.

Results

Characterization of *IaNaR*

Fig 1 shows the sequence of *IaNaR* aligned with the sequences of KR2, another NaR from marine flavobacterium. They were 86% homologous and consisted of 7 domains with each transmembrane helix (TMD1-7).

To study the ion-transport selectivity of *IaNaR*, the protein was expressed in *E. coli* cells and the light-induced pH change was monitored upon illumination of the cell suspension. Fig 2A shows the light-induced pH change of the cell suspension in 100 mM NaCl. We observed an increase in pH (Fig 2A, blue line) that was enhanced by the addition of carbonylcyanide-*m*-chlorophenylhydrazone (CCCP) (Fig 2A, green line). This result indicates that the increase in pH represents the secondary H⁺-uptake into the *E. coli* cell body to compensate the hyperpolarized membrane potential generated by the transport of ions other than H⁺ by *IaNaR*. In order to reveal the type of ion transported by *IaNaR*, we investigated the cation and anion

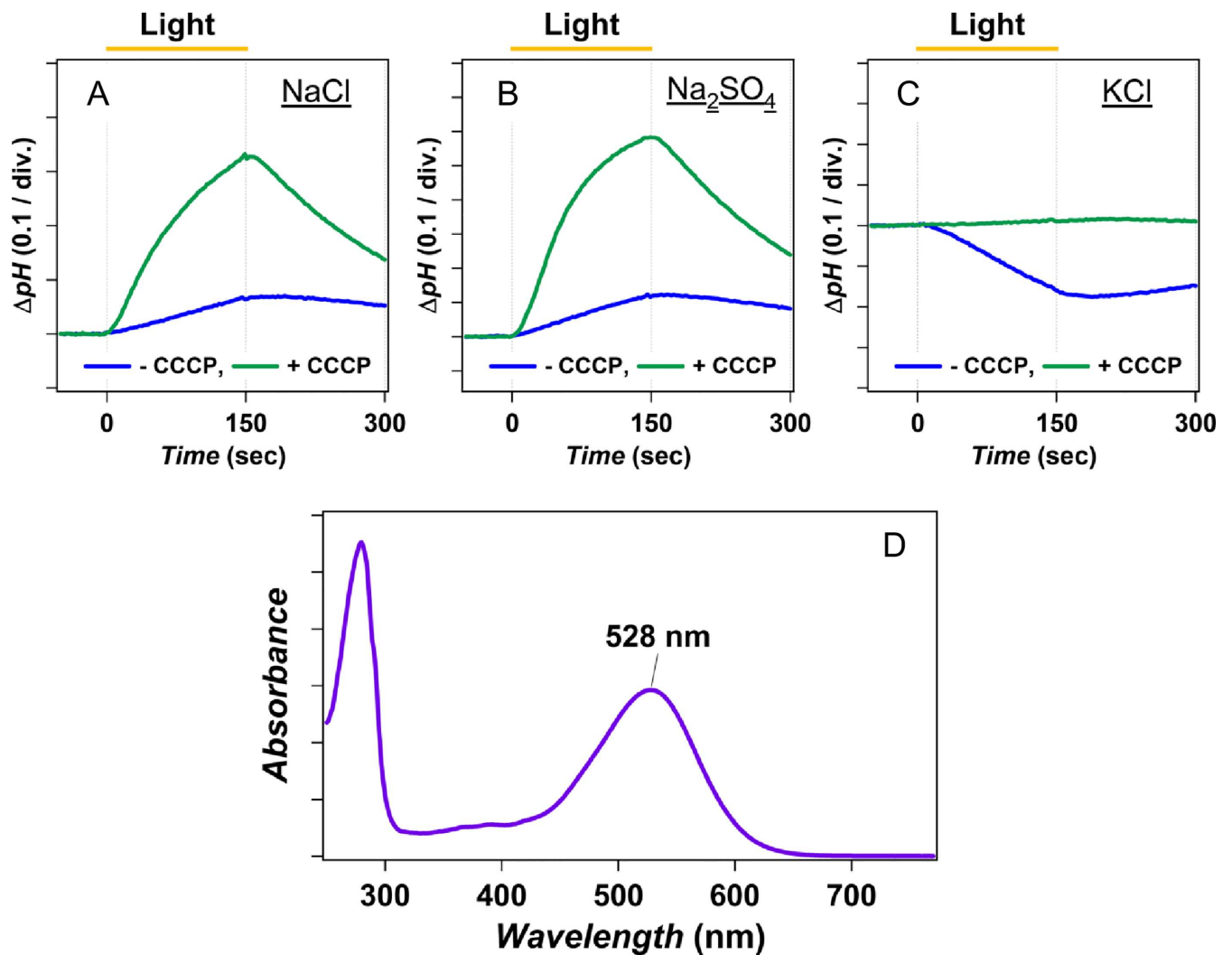


Fig 2. Ion-transport activity of *IaNaR*. (A-C) Light-induced pH changes upon light-illumination (>500 nm, indicated by yellow lines) of the *E. coli* cells expressing *IaNaR* in 100 mM NaCl (A), 100 mM Na₂SO₄ (B) and 100 mM KCl (C) without (blue lines) and with CCCP (green lines). (D) The UV-visible absorption spectrum of purified *IaNaR*.

doi:10.1371/journal.pone.0166820.g002

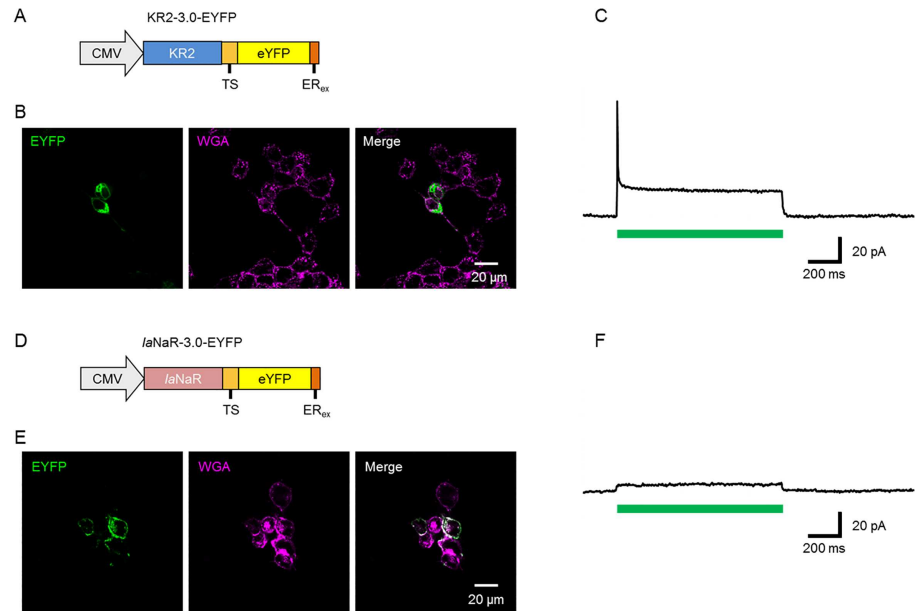


Fig 3. NaR expression in mammalian cells. (A) The expression plasmid, KR2-3.0-eYFP, consisted of the KR2 gene fused with a 20-amino-acid membrane-traffic signal (TS), enhanced yellow fluorescent protein (eYFP), and 7-amino-acid ER-export signal (ER_{ex}). (B) Expression of KR2-3.0-eYFP in the cultured ND7/23 cells: eYFP fluorescence (left, green), wheat germ agglutinin (WGA) conjugated with Alexa Fluor 633 (middle, magenta) and the merge (right). (C) Typical photocurrent of KR2. The green bar indicates the period when green-yellow light (534–600 nm, 99 mW/mm²) was irradiated. (D) The expression plasmid, *IaNAR*-3.0-eYFP. (E) Expression of *IaNAR*-3.0-eYFP in the cultured ND7/23 cells: eYFP fluorescence (left, green), WGA (middle, magenta) and the merge (right). (F) Typical photocurrent of *IaNAR*. The green bar indicates the period when green-yellow light (534–600 nm, 99 mW/mm²) was irradiated.

doi:10.1371/journal.pone.0166820.g003

dependencies. In 100 mM Na₂SO₄, an increase in the pH identical to the result with NaCl was observed (Fig 2B). Thus, the transport of *IaNAR* does not depend on the type of anion in the suspension. By contrast, a decrease in pH was observed in the suspension containing 100 mM KCl (Fig 2C). Because it diminished with the addition of CCCP (Fig 2C, green line), this result shows that *IaNAR* pumps H⁺ in the presence of larger cations. This cation dependence of *IaNAR* is identical to KR2 [26] suggesting that *IaNAR* is a light-driven Na⁺ pump as expected from its amino-acid sequence including the characteristic NDQ-motif which is composed of Asn¹¹¹, Asp¹¹⁵ and Gln¹²² for *IaNAR* [26].

To obtain the absorption spectrum of *IaNAR*, we purified the protein expressed by *E. coli* and solubilized in n-dodecyl-β-D-maltoside (DDM). The spectrum of solubilized *IaNAR* (Fig 2D) showed its absorption maximum at λ_{max} = 528 nm, which is close to that of KR2 (λ_{max} = 524 nm) [26] suggesting that their protein structures should be identical.

The photocurrent properties of *IaNAR* were compared with KR2 by introducing a KR2 gene or *IaNAR* gene fused with membrane-traffic signal (TS), enhanced yellow fluorescent protein (eYFP), and ER-export signal (ER_{ex}) [29] into cultured ND7/23 cells, hybrid cell lines derived from neonatal rat dorsal root ganglia neurons fused with mouse neuroblastoma [31]. The constructs were termed KR2-3.0-eYFP and *IaNAR*-3.0-eYFP, respectively (Fig 3A and 3D). As shown in Fig 3B, the eYFP fluorescence was frequently found in the inclusion bodies in the KR2-expressing cells, suggesting the accumulation of misfolded/mistargeted proteins. However, every expressing cell responded to green-yellow light (534–600 nm, 99 mW/mm²) robustly with an outward photocurrent under a whole-cell clamp at a holding potential of 0 mV (Fig 3C). The KR2 photocurrent was rapidly activated to form a peak current (I_p,

4.26 ± 0.97 pA/pF, n = 10), inactivated to form a steady-state current (I_{ss} , 0.96 ± 0.20 pA/pF, n = 10) and deactivated to the baseline. As ND7/23 cells were live cell-stained with fluorescent WGA, the white merge indicated that the *IaNaR* was mostly expressed in the membrane (Fig 3E). However, its photocurrent generated by green-yellow light (534–600 nm, 99 mWmm⁻²) was significantly smaller than that of KR2 for both I_p (0.22 ± 0.05 pA/pF, n = 10) and I_{ss} (0.19 ± 0.05 pA/pF, n = 10) ($P < 0.005$, Mann-Whitney *U*-test) (Fig 3F). Therefore, KR2 appears to be advantageous for optogenetic applications with larger photocurrent whereas *IaNaR* is suitable for the exogenous expression with better membrane-targeting.

Evaluation of chimeric NaRs

The above results suggested the possibility that some chimeric NaRs between KR2 and *IaNaR* may have the advantages of both NaRs, a larger photocurrent and improved membrane-targeting. To test this, six chimeric NaRs were made by replacing the N-terminal TMDs of KR2 with their counterparts of *IaNaR* (Fig 1) on the assumption that the N-terminal domains of *IaNaR* should be involved in the membrane-targeting. Each gene of chimeric NaR: I_1K_6NaR consisting of TMD1 from *IaNaR* and TMD2-7 from KR2, I_2K_5NaR consisting of TMD1-2 from *IaNaR* and TMD3-7 from KR2, I_3K_4NaR consisting of TMD1-3 from *IaNaR* and TMD4-7 from KR2, I_4K_3NaR consisting of TMD1-4 from *IaNaR* and TMD5-7 from KR2, I_5K_2NaR consisting of TMD1-5 from *IaNaR* and TMD6-7 from KR2 and I_6K_1NaR consisting of TMD1-6 from *IaNaR* and TMD7 from KR2, was fused with TS, eYFP and ER_{ex} and transfected to ND7/23 cells for the evaluation. Since TMD3 of *IaNaR* and KR2 are completely identical to each other (Fig 1), I_2K_5NaR and I_3K_4NaR were the same in the amino-acid sequence but different as genes in the DNA sequence. As shown in Fig 4, the fluorescence expression of each chimeric NaR was similar to that of *IaNaR*. Both the I_p and I_{ss} of I_1K_6NaR were significantly larger than those of the other chimeric NaRs as well as that of *IaNaR* (Fig 5A). Therefore, I_1K_6NaR appeared to be a candidate chimeric NaR for optogenetic applications.

Next, we compared the photocurrent properties of I_1K_6NaR with those of KR2 at the maximal irradiance (534–600 nm, 99 mW/mm²) and at a holding potential of 0 mV (Table 1). Similar to *IaNaR*, the magnitude of inactivation of the I_1K_6NaR photocurrent was significantly smaller than KR2 ($P < 0.005$, Mann-Whitney *U*-test). It was also smaller than those of the other chimeric NaRs (Fig 5B). In the case of KR2, the I_p was monotonically increased with the increase of irradiance, whereas the I_{ss} had a tendency to reach the ceiling at around 20 mW/mm² and was somewhat reduced with the increase of irradiance (Fig 6A and 6C). On the other hand, both the I_p and I_{ss} approached their ceilings with the increase of irradiance in the case of I_1K_6NaR (Fig 6B and 6D). The photocurrent-irradiance relationship is expected to follow Michaelis-Menten kinetics as the rhodopsin follows a single-photon photodynamism [32]. The apparent K_D of I_p was significantly smaller for I_1K_6NaR than for KR2 (Table 1, $P < 0.05$, Mann-Whitney *U*-test). Although the I_{ss} of I_1K_6NaR mostly followed the Michaelis-Menten relationship up to 99 mW/mm², that of KR2 was well fitted to the Michaelis-Menten relationship from which a power-dependent current suppression component above a threshold of 10 mW/mm² was subtracted. Therefore the K_D of I_{ss} was compared by fitting the data of irradiance between 0 and 12 mW/mm² to the Michaelis-Menten relationship. The K_D of I_{ss} was significantly smaller for I_1K_6NaR than for KR2 (Table 1, $P < 0.05$, Mann-Whitney *U*-test).

The I_1K_6NaR photocurrent differed from the KR2 photocurrent in the voltage sensitivity (Fig 7A and 7B). When normalized by the value at a holding potential of 0 mV, the I_p current-voltage (*I-V*) relationship was positively related to the holding potential for both NaRs (Fig 7C). Although the I_{ss} of KR2 was almost insensitive to the holding potential, particularly in the negative region, that of I_1K_6NaR was positively related to the holding potential (Fig 7D). To

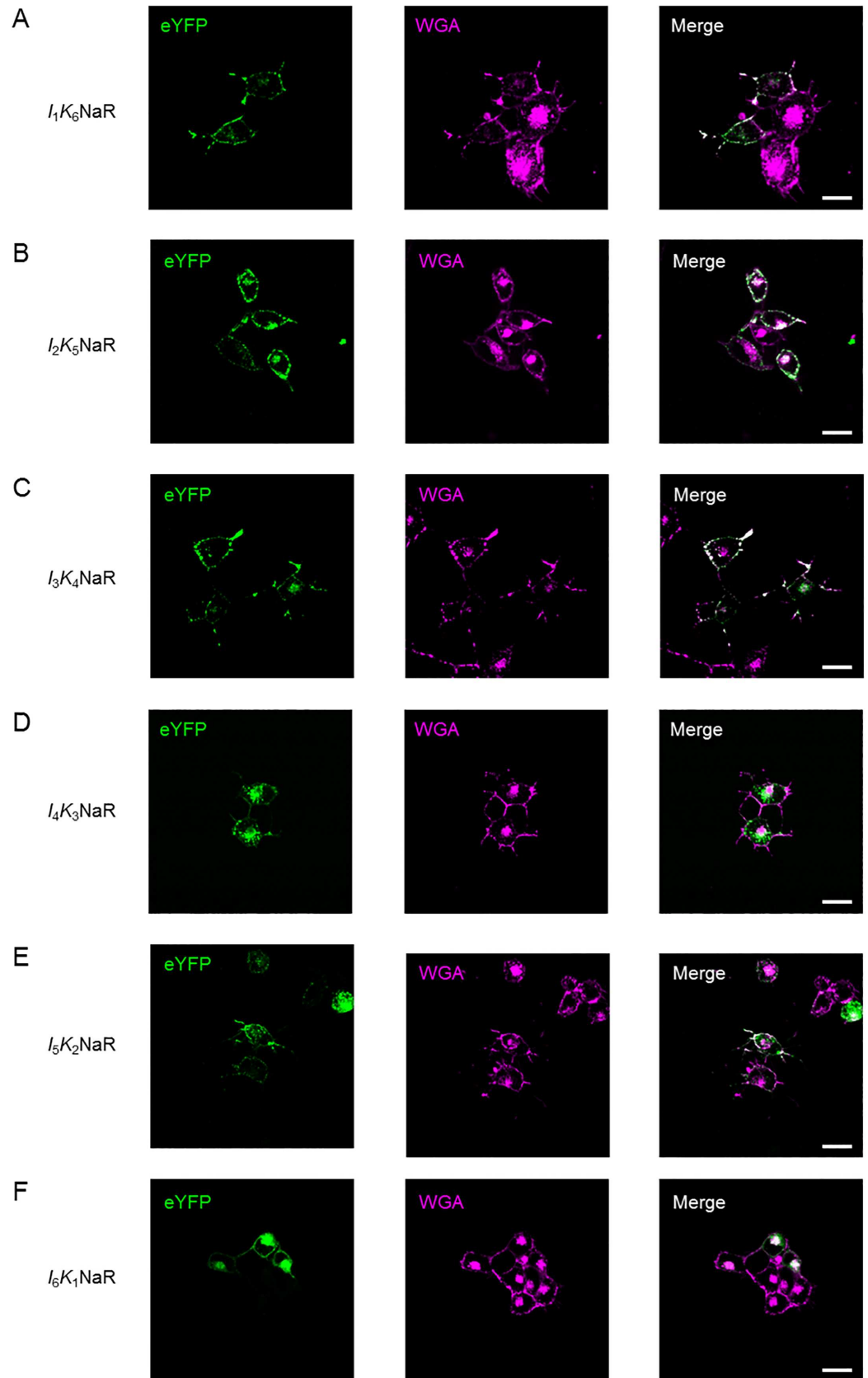


Fig 4. Expression of chimeric NaRs in ND7/23 cells. (A) I_1K_6 NaR: eYFP fluorescence (left), fluorescent wheat germ agglutinin (WGA, middle) and the merge (right). (B)-(F) Similar to (A), but the expression pattern of I_2K_5 NaR, I_3K_4 NaR, I_4K_3 NaR, I_5K_2 NaR, I_6K_1 NaR, respectively. Scale, 20 μ m for each.

doi:10.1371/journal.pone.0166820.g004

further test this, the slope of each normalized I - V relationship was calculated in the negative region of the holding potential (S_{neg}). As shown in Table 1, the S_{neg} of I_1K_6 NaR was significantly larger than that of KR2 for I_{ss} ($P < 0.005$, Mann-Whitney U -test) but not for I_p .

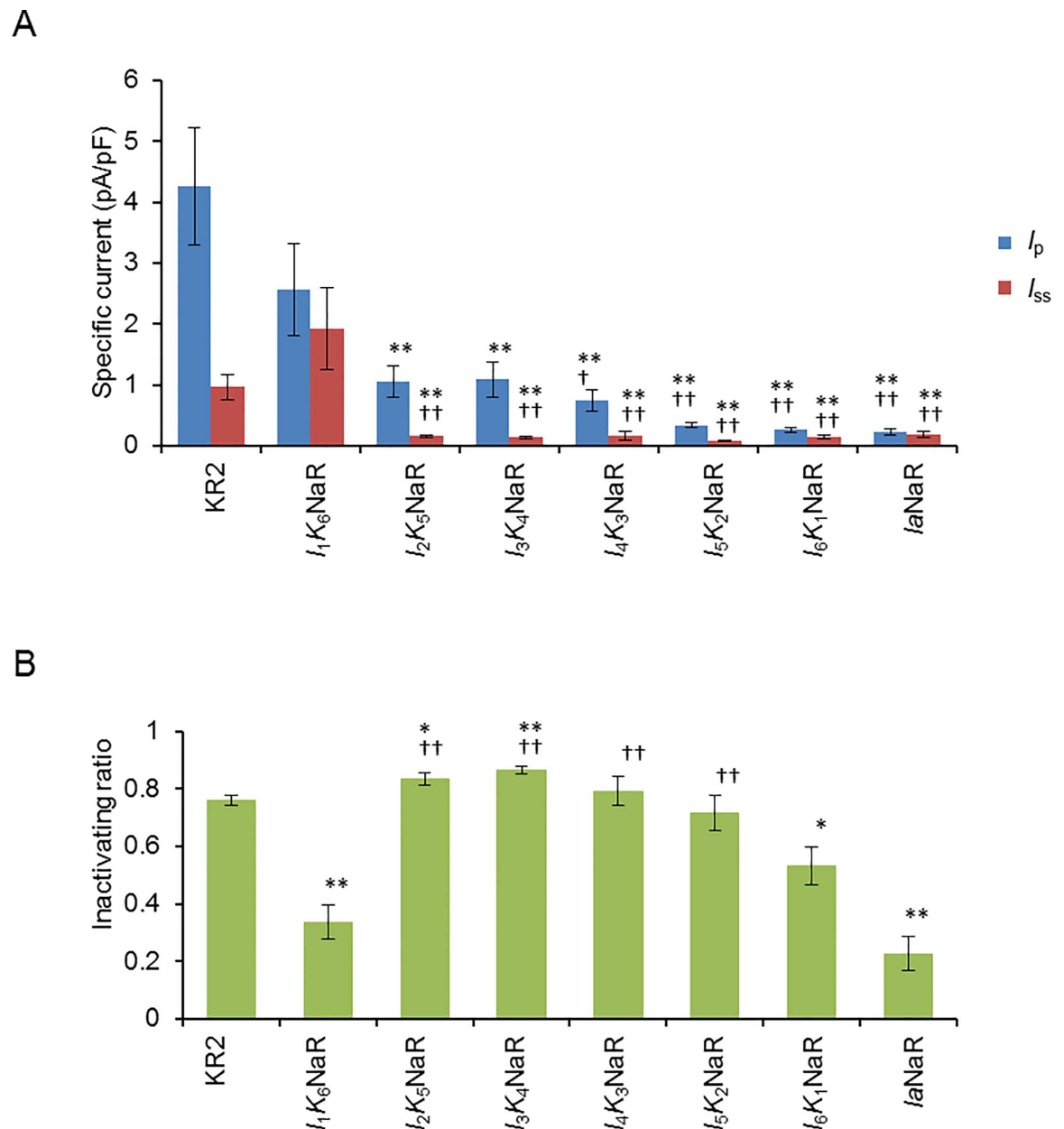


Fig 5. Photocurrent of chimeric NaRs. (A) The peak (I_p , blue columns) and the steady-state (I_{ss} , red columns) photocurrent at 0 mV holding potential in response to green-yellow light (534–600 nm, 99 mW/mm²) were compared among KR2 (n = 10), chimeric NaRs: I_1K_6 NaR (n = 11), I_2K_5 NaR (n = 10), I_3K_4 NaR (n = 10), I_4K_3 NaR (n = 10), I_5K_2 NaR (n = 10), I_6K_1 NaR (n = 9) and I_a NaR (n = 10). (B) Comparison of the inactivating ratio. The difference was significant when compared to KR2 (*, $P < 0.05$, **, $P < 0.005$, Mann-Whitney U -test) or I_1K_6 NaR (\dagger , $P < 0.05$, $\dagger\dagger$, $P < 0.005$, Mann-Whitney U -test).

doi:10.1371/journal.pone.0166820.g005

Table 1. Photocurrent characteristics of KR2 and I₁K₆NaR.

	KR2	I ₁ K ₆ NaR
I _p [pA/pF]	4.26 ± 0.97 (n = 10)	**2.57 ± 0.75 (n = 11)
I _{ss} [pA/pF]	0.96 ± 0.20 (n = 10)	**1.92 ± 0.68 (n = 11)
Inactivation ratio	0.76 ± 0.02 (n = 10)	**0.34 ± 0.06 (n = 11)
K _D (I _p) [mW/mm ²]	39.3 ± 8.3 (n = 8)	*8.3 ± 1.1 (n = 9)
K _D (I _{ss}) [mW/mm ²]	18.7 ± 4.9 (n = 8)	*6.2 ± 1.4 (n = 9)
S _{neg} (I _p) [10 ³ mV ⁻¹]	4.03 ± 0.39 (n = 8)	2.45 ± 0.90 (n = 7)
S _{neg} (I _{ss}) [10 ³ mV ⁻¹]	0.43 ± 1.00 (n = 8)	**7.33 ± 2.13 (n = 7)

The photocurrents were responses to green-yellow light (534–600 nm) at 99 mW/mm² except for K_D for which the power of light was variable.

*, P < 0.05

**, P < 0.005

Mann-Whitney U-test

doi:10.1371/journal.pone.0166820.t001

The I_{ss} at each wavelengths (390, 438, 475, 513, 549, 575 and 632 nm at the center, respectively) was corrected by the irradiance (3.4, 3.0, 2.7, 2.7, 2.6, 2.8 and 2.8 mW/mm², respectively) and its relative sensitivity to the maximum was averaged for KR2 and I₁K₆NaR and shown in Fig 8 as a function of the wavelength. Although the spectral sensitivity of the I₁K₆NaR photocurrent was almost similar to that of KR2, it was significantly lower in response to yellow light (575 nm) (P < 0.005, Mann-Whitney U-test).

Light-dependent inhibition of neuronal activity

Previously, the light-dependent activation of KR2 effectively silenced the neural activities both *in vitro* and *in vivo*. To test the possible application of I₁K₆NaR as an optogenetic silencer, the light-dependent changes of the membrane potential were investigated in cultured rat cortical neurons expressing I₁K₆NaR. As shown in Fig 9A, the I₁K₆NaR fluorescence was localized in the membrane when expressed in the cultured cortical neurons. Quantitative comparisons of the membrane targeting of the eYFP-labeled molecules were made between I₁K₆NaR and KR2 using primary cultured neurons from the cortex the plasma membrane of which was live cell-stained with a fluorescence marker, Alexa Fluor 633-labeled WGA. For each molecule, 10 neurons were randomly selected and the confocal images of their somas were quantitatively analyzed for localization of the fluorescence; the overlapping index of I₁K₆NaR was 0.38 ± 0.06 (n = 10) and positive for every neuron (range, 0.11~0.68) (Fig 9B). On the other hand, the overlapping index of KR2 fluorescence was -0.10 ± 0.06 (n = 10), negative in 7 of 10 neurons (range, -0.53~0.24) and significantly smaller than that of I₁K₆NaR (P < 0.0005, Mann-Whitney U-test) (Fig 9C and 9D).

Under current clamp, the resting membrane potentials (RMPs) were between -51 and -83 mV (-64 ± 4 mV, n = 11) and hyperpolarized by 8–24 mV (-15 ± 5 mV, n = 11) with light (549 nm, 2.6 mW/mm²). Although action potentials were repetitively generated by the depolarization through current injection, they were hardly evoked during irradiation of light (Fig 10A). In every experiment (n = 11), the action potentials, evoked once, were reversibly inhibited during irradiation (549 nm, 2.6 mW/mm²). The light-induced inhibition of firing was quite stable and remained effective for as long as 10 s (Fig 10B–10D). In summary of 7 similar experiments (Fig 10E), the firing frequency was significantly smaller throughout the irradiation period (10 s, 549 nm, 2.6 mW/mm²) than the corresponding period in the darkness (P < 0.05, Wilcoxon signed rank test). The firing frequency was often increased when the irradiation was

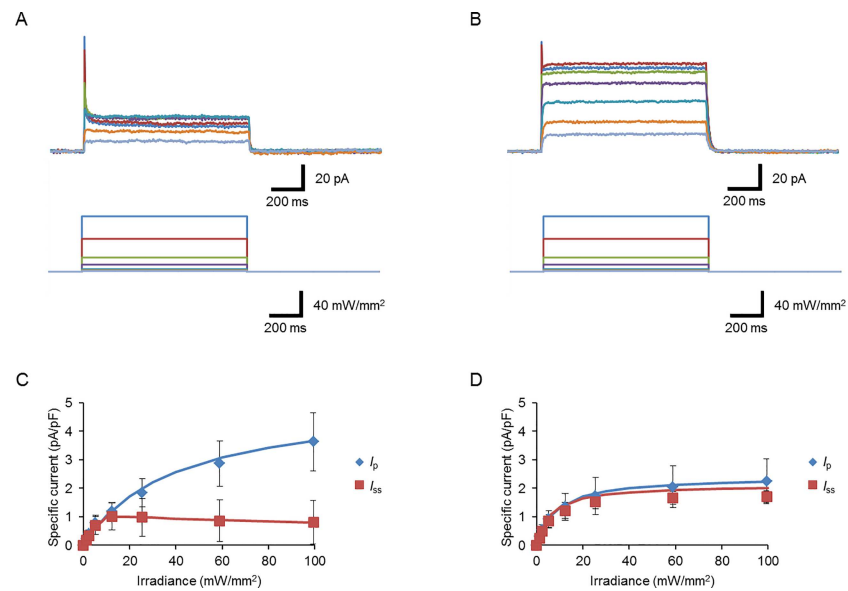


Fig 6. Photocurrent properties of I₁K₆NaR. (A) Sample photocurrents of KR2 (upper traces) at various powers of light (lower traces). (B) Sample photocurrents of I₁K₆NaR (upper traces) at various powers of light (lower traces). (C) The amplitude of the peak (I_p, blue diamonds) and steady-state (I_{ss}, red squares) of the KR2 photocurrents as functions of irradiance (n = 8). The blue line is drawn according to the Michaelis-Menten relationship, $y = 5.12x/(x+39.3)$. The red line is the Michaelis-Menten relationship from which the power-dependent current suppression component above a threshold of 10 mW/mm² was subtracted, $y = 2.8x/(x + 18.7) - 2.3(x-10)/\{(x-10)+38.1\}$. (D) Similar to (C), but in the case of I₁K₆NaR photocurrent (n = 9). Each line is drawn according to the Michaelis-Menten relationship, $y = 2.4x/(x+8.3)$ (blue) and, $y = 2.1x/(x+6.2)$ (red), respectively.

doi:10.1371/journal.pone.0166820.g006

turned off (rebound potentiation, Fig 10C and 10D). Indeed, a significant increase of firing frequency was observed in 4 of 7 similar experiments (Fig 10E).

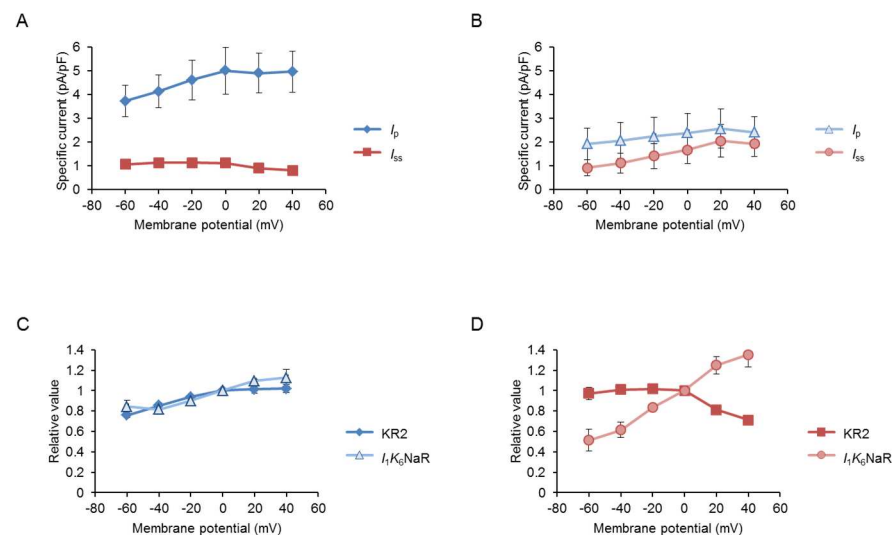


Fig 7. Sensitivity of I₁K₆NaR photocurrent to the membrane potential. (A) The current-voltage (I-V) relationship of the peak (I_p, blue diamonds) and steady-state (I_{ss}, red squares) of the KR2 photocurrents (n = 8). (B) The current-voltage (I-V) relationship of peak (I_p, light blue triangles) and steady-state (I_{ss}, light red circles) of I₁K₆NaR photocurrents (n = 7). (C) Each I_p of KR2 (blue diamond) and I₁K₆NaR (light blue triangle) was expressed as a relative value to that at 0 mV holding potential and plotted as a function of voltage. (D) Each I_{ss} of KR2 (red square) and I₁K₆NaR (light red circle) was expressed as a relative value to that at 0 mV holding potential and plotted as a function of voltage.

doi:10.1371/journal.pone.0166820.g007

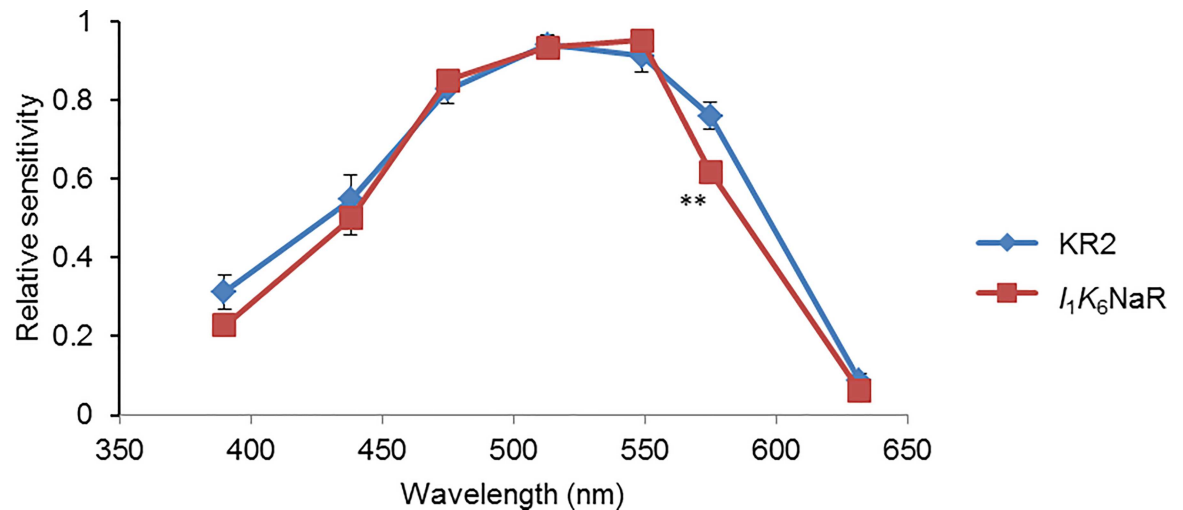


Fig 8. Action spectrum of I₁K₆NaR. For each wavelength the relative photocurrent amplitude (I_{ss}) was divided by the irradiance, normalized to its maximum and averaged. The photocurrents of KR2 (blue diamonds, $n = 9$) and I₁K₆NaR (red squares, $n = 12$) did not show transient peaks because of the small magnitude of irradiance. **, $P < 0.005$, Mann-Whitney U -test.

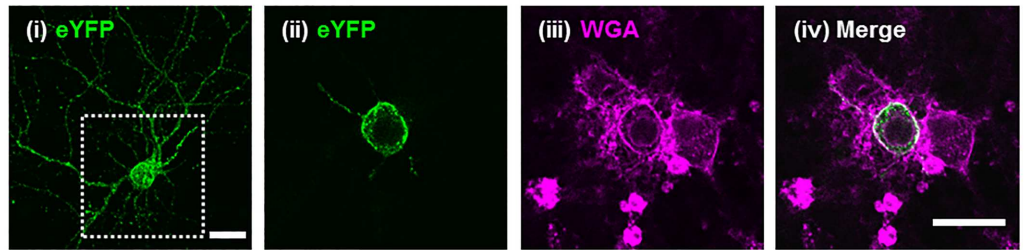
doi:10.1371/journal.pone.0166820.g008

Discussion

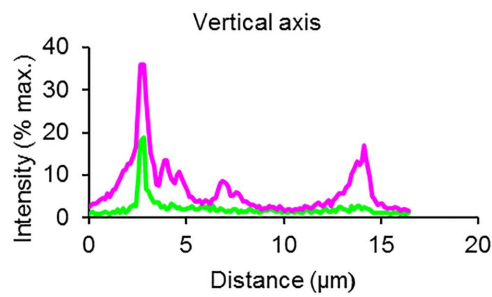
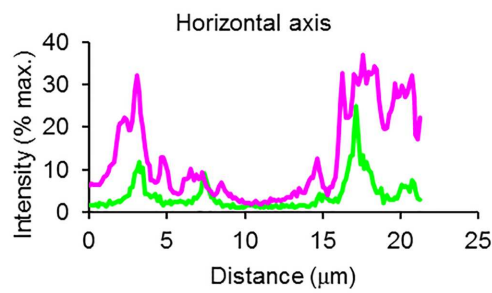
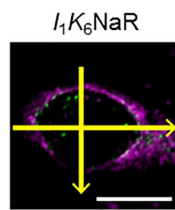
This study addressed the question whether a new Na⁺-pump rhodopsin from *Indibacter alkaliophilus* (*IaNaR*) could serve as an optogenetic silencer with negligible disturbance of the ionic milieu both inside and outside of the membrane [27]. The ion-transport assay with *E. coli* cells showed that *IaNaR* outwardly transports Na⁺ when the internal solution contained Na⁺, but H⁺ when all the Na⁺ was replaced by K⁺. This ion-transporting property and selectivity is identical to KR2, the first reported NaR [26], and NaR from *Dokdonia sp.* PRO95 [33]. λ_{max} of *IaNaR* (528 nm) is also similar to KR2 (524 nm) [26] and NaR from *Dokdonia sp.* PRO95. (523 nm) [33]. Therefore, the fundamental properties of *IaNaR* including the ion-transporting function and the structure around retinal are similar of those of previously reported NaRs. When *IaNaR* was expressed in the mammalian cells such as ND7/23, its photocurrent was very small even under the maximal power of green-yellow light (534–600 nm, 99 mW/mm²). However, it appeared to be better targeted to the plasma membrane than KR2.

The eYFP-labeled KR2 molecules frequently accumulated in large intracellular compartments even after the gene was fused with a TS and an ER_{ex} which facilitates the plasma membrane expression of the transcribed rhodopsins [29]. The exogenously expressed membrane proteins are often misfolded resulting in the ER retention or degradation with a reduction of functional membrane proteins at their correct sites [34]. The accumulation of misfolded proteins also causes ER stress, which can lead to cell death if remains unmitigated [35,36]. It is possible that *IaNaR* could provide conformations that help the rhodopsin to become folded correctly and to be targeted to the plasma membrane with minimal ER stress. Indeed, the chimera rhodopsins consisting of the N-terminal TMDs from *IaNaR* and the C-terminal TMDs of KR2 appeared to be well targeted to the plasma membrane rather than in the intracellular compartments of ND7/23 cells. Among the chimeras, I₁K₆NaR consisting of TMD1 from *IaNaR* and TMD2-7 from KR2 generated I_p and I_{ss} as large as KR2. However, it remains puzzling that the magnitude of the photocurrent of *IaNaR* and some of its chimeric derivatives was similar to or lower than that of KR2 even with the improved membrane targeting. The possibility that the ion-transporting efficiency of *IaNaR* and its derivatives is lower than that of KR2

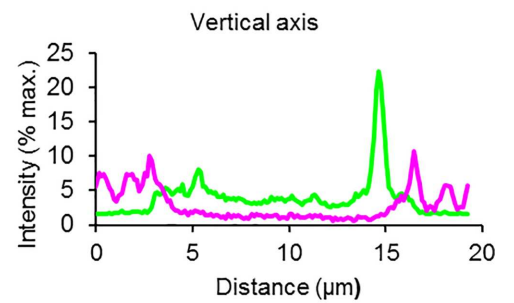
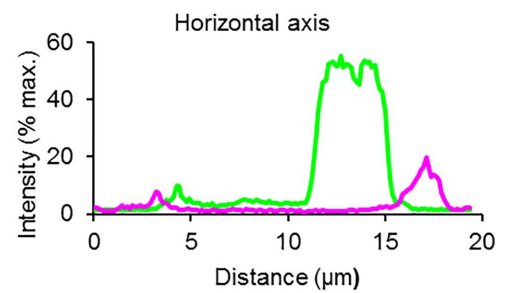
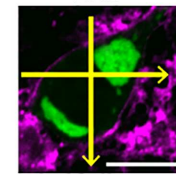
A



B



C



D

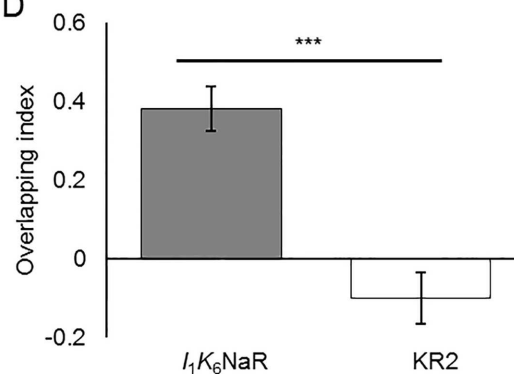


Fig 9. Quantitative evaluation of membrane targeting of NaRs. (A) Expression of eYFP-labeled I_1K_6 NaR in the cultured cortical neuron. (i) Integrated confocal image of the neuron (Z-stack projection of 12 slices at every 0.46 μ m in depth). (ii) eYFP image of a single slice shown in the dot-lined square in (i). (iii) Image of the fluorescent WGA of the same region. (iv) Merge of (ii) and (iii), indicating the expression of I_1K_6 NaR in the neuronal membrane. (B) Profiling of the fluorescent intensity of an I_1K_6 NaR-expressing neuron. The pixel values along the horizontal/vertical axes, which were delineated to pass the centroid of the cell (yellow), were plotted as functions of distance: eYFP fluorescence (green) and WGA fluorescence (magenta). The overlapping index was 0.68. (C) Profiling of the fluorescent intensity for a KR2-expressing neuron. The overlapping index was -0.21. (D) Comparison of the overlapping index between I_1K_6 NaR (left) and KR2 (right). ***, $P < 0.0005$, Mann-Whitney U -test. Scales, 20 μ m for (A) and 10 μ m for (B) and (C).

doi:10.1371/journal.pone.0166820.g009

should be investigated in future. Alternatively, the membrane-targeted molecules may be relatively rapidly internalized and/or denatured in the case of Ia NaR and its derivatives. Further modification of molecules, focusing on the N-terminal extracellular segment and TM1, might create a NaR with larger photocurrent amplitude and better membrane targeting [37–39].

Similar to KR2, the ion-transport assay with *E. coli* cells showed that I_1K_6 NaR outwardly transports Na⁺ when the internal solution contained Na⁺, but H⁺ when all Na⁺ was replaced by K⁺ (S1 Fig). However, the photocurrent properties of I_1K_6 NaR were somewhat different from those of KR2. Although the difference was insignificant, the I_{ss} of I_1K_6 NaR was relatively large but with a significantly smaller inactivation ratio. The I_1K_6 NaR was significantly more sensitive to light (534–600 nm) than KR2 in both I_p and I_{ss} . As the spectral sensitivity of I_1K_6 NaR was similar to KR2, the different sensitivity may be attributed to the probability of conformational changes at the molecular level upon light absorption. Although KR2 photocurrent was almost insensitive to voltage in both I_p and I_{ss} as reported previously [27], the I_{ss} of I_1K_6 NaR was positively related to the voltage. These photocurrent properties as well as its membrane-targeting trait would suggest that I_1K_6 NaR could become one of the optogenetic NaRs for long-term silencing of neural activities with relatively low power of light.

Upon the cessation of light exposure, the rapid recovery of the membrane potential was often accompanied by the rebound potentiation with the possible changes in the membrane properties during hyperpolarization: the reduced inactivation of voltage-dependent Na⁺ channels, the deactivation of voltage-dependent K⁺ channels, and the activation of HCN channels (I_h). Indeed, the NaR-dependent neural silencing was often accompanied by an increase in the firing frequency upon termination of light pulse. Although NpHR and AR3/ArchT are widely used optogenetic tools for neural silencing, they still have much room for improvement. For example, several papers reported that NpHR triggers artificial neural spiking relatively long after turning-off the light [40–42]. As intracellular Cl⁻ accumulation would inevitably accompany the positive shift of the Cl⁻-equilibrium potential, it is reasonable to assume that the Cl⁻ pumping activity of NpHR enhances the magnitude and duration of the rebound potentiation. In addition, this Cl⁻ accumulation may not be a trivial problem in some cases, such as *in vivo* optogenetic analysis of mammalian neurons during developmental stages. In adult mammals, the intracellular Cl⁻ concentration is maintained at a low level by several transporters, such as KCC2. However, in developmental stages, when the Cl⁻ extrusion system is still immature, the intracellular Cl⁻ concentration is relatively high with depolarized Cl⁻ equilibrium potential [43,44]. Similarly, it is assumed that the intracellular Cl⁻ accumulation by the activity of the light-driven Cl⁻ pump further enhances the magnitude and duration of the rebound potentiation with repetitive firing, and makes it difficult to infer the functions of target neurons and neural circuits in the behavioral response [45]. In the case of AR3/ArchT, the light-dependent change of local pH around the neurons can activate the proton-gated cation channel such as ASIC (acid sensing ion channel) and cause unintentional rebound potentiation [46]. The AR3/ArchT-dependent intracellular alkalinization may lead to the unintentional release of

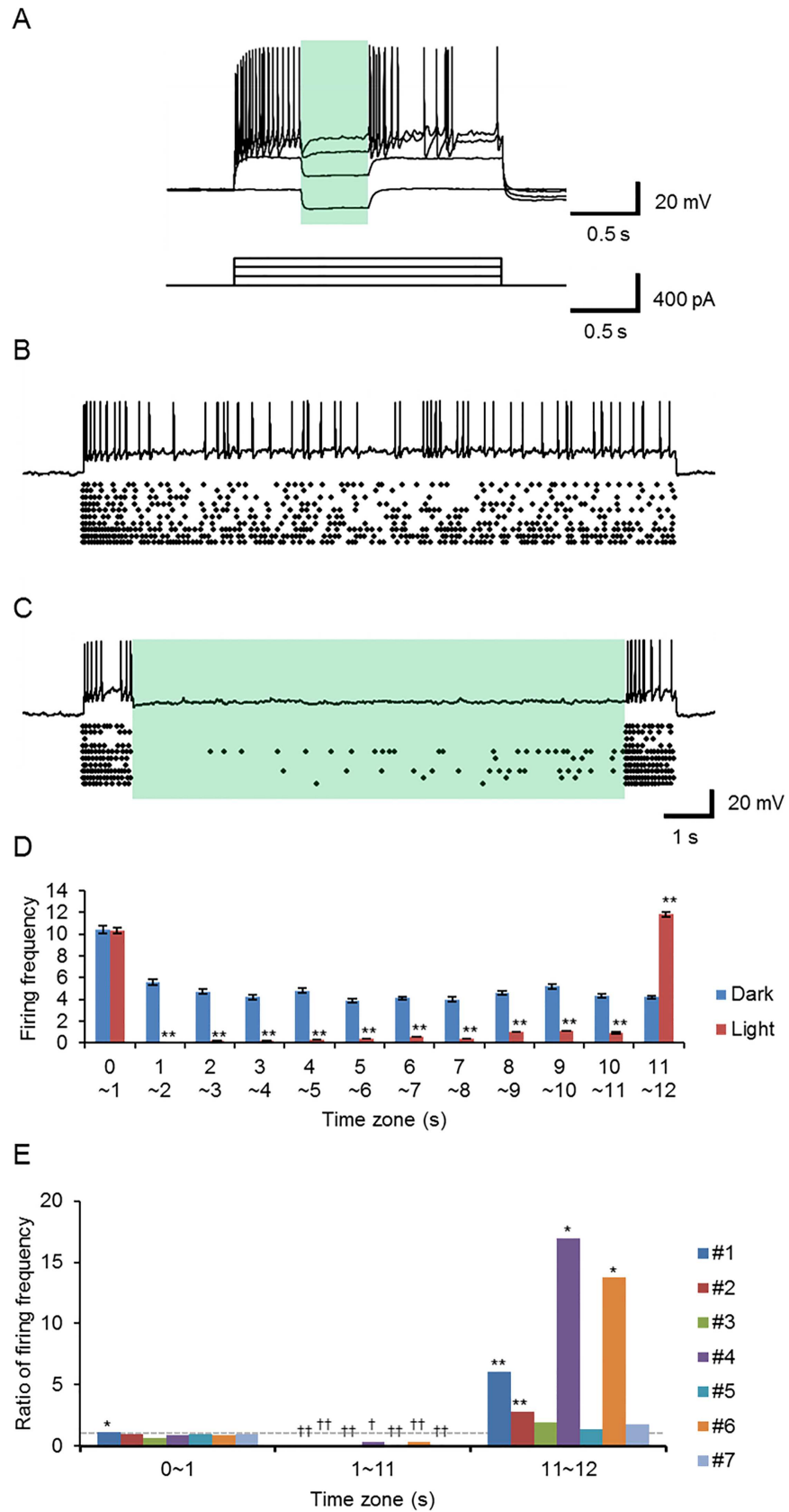


Fig 10. Light-dependent silencing of the neuronal activity. (A) Series of sample records of the membrane potentials of an I_1K_6 NaR-expressing neuron under current clamp (top traces, RMP, -76 mV). The depolarization was made through current injection (bottom traces). The green light (549 nm, 2.6 mW/mm²) hyperpolarized the membrane potential and suppressed the generation of action potentials. (B) Generation of repetitive action potentials in an I_1K_6 NaR-expressing neuron under current clamp (top trace, RMP, -73 mV). The responses to 10 repetitive depolarizations are summarized as raster plots of the action potentials (bottom). (C) The activity of the same neuron was stably silenced during the green light irradiation (549 nm, 2.6 mW/mm²) for 10 s (top trace, RMP, -73 mV). The responses to 10 repetitive depolarizations are summarized as raster plots of action potentials (bottom). (D) The firing frequencies during time zones of 1 s each. The effects of green light irradiation (time zones from 2–11 s) were compared for the same neuron shown in (A) and (B); without ('Dark' protocol, blue columns) and with light ('Light' protocol, red columns). Note the significant increase of firing frequency at the off period (time zone 11–12 s). (E) Ratios of firing frequency of 'Light' to 'Dark' protocol during time zone 0–1 s (before irradiation), 1–11 s (during irradiation), 11–12 s (after irradiation), respectively for each neuron #1–7 expressing I_1K_6 NaR (experimental order). The gray dotted line indicate that the ratio = 1. *, $P < 0.05$; **, $P < 0.005$; Mann-Whitney U -test applied to the set of records. †, $P < 0.05$; ††, $P < 0.005$; Wilcoxon signed rank test applied to the firing frequency for time zone, 1–2, 2–3, 3–4, 4–5, 5–6, 6–7, 7–8, 8–9, 9–10 and 10–11, respectively.

doi:10.1371/journal.pone.0166820.g010

neurotransmitter through triggering Ca²⁺ influx [47]. Similar cautions will be necessary in the case of light-gated Cl⁻/anion channels [12–15] as the direction of membrane potential change is dependent on the equilibrium potential of Cl⁻ that can be affected by many factors such as development, localization and disease [18–25]. Distinct from the Cl⁻/anion channel rhodopsins, the hyperpolarization of the membrane potential is always expected for any NaR because of the unidirectional transport of Na⁺. Indeed the I_1K_6 NaR-expressing cortical neurons were stably silenced by green light irradiation for a rather long duration. In addition, the artefactual change of the pH balance is expected to be almost negligible as the H⁺-transporting rate is estimated to be less than 3% those of Na⁺. This estimation based on the higher Na⁺ activity than H⁺ (320,000-fold) inside a mammalian cell in a physiological condition such as 10 mM Na⁺ and pH 7.3, whereas the rate constant of H⁺ uptake was larger than that of Na⁺ uptake with a ratio of 8,000–9000 [48]. Furthermore, one of the marked advantages of I_1K_6 NaR is its I - V relationship: the photocurrent is smaller at the resting membrane potential while larger at the depolarized potential. Under the current-clamp condition, the outward transport of Na⁺ by the irradiated I_1K_6 NaR is increased by the depolarization before generation of the action potential. As a result, the action potential is inhibited and the membrane potential is hyperpolarized, which on the other hand, decreases the outward Na⁺ flow. Therefore, with its rapid kinetics, the photoactivation of I_1K_6 NaR could become an ideal optogenetic silencer that specifically suppresses the generation of action potentials with less hyperpolarization of the neuronal membrane potential than KR2. Since the rebound potentiation is dependent on the magnitude of the hyperpolarization and on the duration, its magnitude is expected to be less for I_1K_6 NaR.

Conclusions

We found that one of the chimeras between KR2 and I_a NaR, named I_1K_6 NaR, exhibited some improvements in membrane targeting and photocurrent properties over native NaRs. The I_1K_6 NaR would be a potential candidate of the effective optogenetic neural silencer with minimal influence on the ionic/pH balance.

Supporting Information

S1 Fig. Ion-transport activity of I_1K_6 NaR. (a–c) Light-induced pH changes upon light-illumination (>500 nm, indicated by yellow lines) on the *E. coli* cells expressing I_1K_6 NaR in 100 mM NaCl (a), 100 mM Na₂SO₄ (b) and 100 mM KCl (c) without (blue lines) and with CCCP (green lines).

(PDF)

Acknowledgments

We thank S. Hososhima for technical instruction and B. Bell for language assistance.

Author Contributions

Conceptualization: KI HK HY.

Formal analysis: MRH RA-Y HY.

Funding acquisition: TI HY.

Investigation: MRH RA-Y HI.

Methodology: KI TI HY.

Resources: TM.

Writing – original draft: MRH TI KI RA-Y HY.

References

1. Yizhar O, Fenno LE, Davidson TJ, Mogri M, Deisseroth K. Optogenetics in neural systems. *Neuron*. 2011; 71:9–34. doi: [10.1016/j.neuron.2011.06.004](https://doi.org/10.1016/j.neuron.2011.06.004) PMID: [21745635](https://pubmed.ncbi.nlm.nih.gov/21745635/)
2. Yawo H, Asano T, Sakai S, Ishizuka T. Optogenetic manipulation of neural and non-neural functions. *Dev Growth Diff*. 2013; 55:474–490. doi: [10.1111/dgd.12053](https://doi.org/10.1111/dgd.12053) PMID: [23550617](https://pubmed.ncbi.nlm.nih.gov/23550617/)
3. Deisseroth K. Optogenetics: 10 years of microbial opsins in neuroscience. *Nat Neurosci*. 2015; 18:1213–1225. doi: [10.1038/nn.4091](https://doi.org/10.1038/nn.4091) PMID: [26308982](https://pubmed.ncbi.nlm.nih.gov/26308982/)
4. Yawo H, Egawa R, Hososhima S, Wen L. Chapter 8. General description: Future prospects of optogenetics. In Yawo H, Kandori H, Koizumi A, editors. *Optogenetics: Light-Sensing Proteins and Their Applications*. Tokyo: Springer; 2015. pp. 111–132.
5. Boyden ES, Zhang F, Bamberg E, Nagel G, Deisseroth K. Millisecond-timescale, genetically targeted optical control of neural activity. *Nat Neurosci*. 2005; 8:1263–1268. doi: [10.1038/nn1525](https://doi.org/10.1038/nn1525) PMID: [16116447](https://pubmed.ncbi.nlm.nih.gov/16116447/)
6. Ishizuka T, Kakuda M, Araki R, Yawo H. Kinetic evaluation of photosensitivity in genetically engineered neurons expressing green algae light-gated channels. *Neurosci Res*. 2006; 54:85–94. doi: [10.1016/j.neures.2005.10.009](https://doi.org/10.1016/j.neures.2005.10.009) PMID: [16298005](https://pubmed.ncbi.nlm.nih.gov/16298005/)
7. Zhang F, Wang LP, Brauner M, Liewald JF, Kay K, Watzke N, et al. Multimodal fast optical interrogation of neural circuitry. *Nature*. 2007; 446:633–639. doi: [10.1038/nature05744](https://doi.org/10.1038/nature05744) PMID: [17410168](https://pubmed.ncbi.nlm.nih.gov/17410168/)
8. Han X, Boyden ES. Multiple-color optical activation, silencing, and desynchronization of neural activity, with single-spike temporal resolution. *PLoS ONE*. 2007; 2:e299. doi: [10.1371/journal.pone.0000299](https://doi.org/10.1371/journal.pone.0000299) PMID: [17375185](https://pubmed.ncbi.nlm.nih.gov/17375185/)
9. Chow BY, Han X, Dobry AS, Qian S, Chuong AS, Li M, et al. High-performance genetically targetable optical neural silencing by light-driven proton pump. *Nature*. 2010; 46:98–102. doi: [10.1038/nature08652](https://doi.org/10.1038/nature08652)
10. Han X, Chow BY, Zhou H, Klapoetke NC, Chuong A, Rajimehr R, et al. A high-light sensitivity optical neural silencer: development and application to optogenetic control of non-human primate cortex. *Front Sys Neurosci*. 2011; 5:00018. doi: [10.3389/fnsys.2011.00018](https://doi.org/10.3389/fnsys.2011.00018) PMID: [21811444](https://pubmed.ncbi.nlm.nih.gov/21811444/)
11. Zhang F, Vieroch J, Yizhar O, Fenno LE, Tsunoda S, Kianianmomeni A, et al. The microbial opsin family of optogenetic tools. *Cell*. 2011; 147:1446–1457. doi: [10.1016/j.cell.2011.12.004](https://doi.org/10.1016/j.cell.2011.12.004) PMID: [22196724](https://pubmed.ncbi.nlm.nih.gov/22196724/)
12. Wietek J, Wiegert JS, Adeishvili N, Schneider F, Watanabe H, Tsunoda SP, et al. Conversion of channelrhodopsin into a light-gated chloride channel. *Science*. 2014; 344:409–412. doi: [10.1126/science.1249375](https://doi.org/10.1126/science.1249375) PMID: [24674867](https://pubmed.ncbi.nlm.nih.gov/24674867/)
13. Berndt A, Lee SY, Ramakrishnan C, Deisseroth K. Structure-guided transformation of channelrhodopsin into a light-activated chloride channel. *Science*. 2014; 344:420–424. doi: [10.1126/science.1252367](https://doi.org/10.1126/science.1252367) PMID: [24763591](https://pubmed.ncbi.nlm.nih.gov/24763591/)
14. Govorunova EG, Sineshchekov OA, Janz R, Liu X, Spudich JL. Natural light-gated anion channels: A family of microbial rhodopsins for advanced optogenetics. *Science*. 2015; 349:647–650. doi: [10.1126/science.aaa7484](https://doi.org/10.1126/science.aaa7484) PMID: [26113638](https://pubmed.ncbi.nlm.nih.gov/26113638/)

15. Berndt A, Lee SY, Wietek J, Ramakrishnan C, Steinberg EE, Rashid AJ, et al. Structural foundations of optogenetics: Determinants of channelrhodopsin ion selectivity. *Proc Natl Acad Sci USA*. 2016; 113:822–829. doi: [10.1073/pnas.1523341113](https://doi.org/10.1073/pnas.1523341113) PMID: [26699459](https://pubmed.ncbi.nlm.nih.gov/26699459/)
16. Beppu K, Sasaki T, Tanaka KF, Yamanaka A, Fukazawa Y, Shigemoto R, et al. Optogenetic countering of glial acidosis suppresses glial glutamate release and ischemic brain damage. *Neuron*. 2014; 81:314–320. doi: [10.1016/j.neuron.2013.11.011](https://doi.org/10.1016/j.neuron.2013.11.011) PMID: [24462096](https://pubmed.ncbi.nlm.nih.gov/24462096/)
17. Alfonsa H, Merricks EM, Codadu NK, Cunningham MO, Deisseroth K, Racca C, et al. The contribution of raised intraneuronal chloride to epileptic network activity. *J Neurosci*. 2015; 35:7715–7726. doi: [10.1523/JNEUROSCI.4105-14.2015](https://doi.org/10.1523/JNEUROSCI.4105-14.2015) PMID: [25995461](https://pubmed.ncbi.nlm.nih.gov/25995461/)
18. Ben-Ari Y. Excitatory actions of gaba during development: the nature of the nurture. *Nat Rev Neurosci*. 2002; 3:728–739. doi: [10.1038/nrn920](https://doi.org/10.1038/nrn920) PMID: [12209121](https://pubmed.ncbi.nlm.nih.gov/12209121/)
19. Ben-Ari Y, Gaiarsa J-L, Tyzio R, Khazipov R. GABA: a pioneer transmitter that excites immature neurons and generates primitive oscillations. *Physiol Rev*. 2007; 87:1215–1284. doi: [10.1152/physrev.00017.2006](https://doi.org/10.1152/physrev.00017.2006) PMID: [17928584](https://pubmed.ncbi.nlm.nih.gov/17928584/)
20. Szabadics J, Varga C, Molnár G, Oláh S, Barzó P, Tamás G. Excitatory effect of GABAergic axo-axonic cells in cortical microcircuits. *Science*. 2006; 311:233–5. doi: [10.1126/science.1121325](https://doi.org/10.1126/science.1121325) PMID: [16410524](https://pubmed.ncbi.nlm.nih.gov/16410524/)
21. Glykys J, Dzhalal V, Egawa K, Balena T, Saponjian Y, Kuchibhotla KV, et al. Local impermeant anions establish the neuronal chloride concentration. *Science*. 2014; 343:670–675. doi: [10.1126/science.1245423](https://doi.org/10.1126/science.1245423) PMID: [24503855](https://pubmed.ncbi.nlm.nih.gov/24503855/)
22. Kaila K, Ruusuvuori E, Seja P, Voipio J, Puskarjov M. GABA actions and ionic plasticity in epilepsy. *Curr Opin Neurobiol*. 2014; 26:34–41. doi: [10.1016/j.conb.2013.11.004](https://doi.org/10.1016/j.conb.2013.11.004) PMID: [24650502](https://pubmed.ncbi.nlm.nih.gov/24650502/)
23. Pond BB, Berglund K, Kuner T, Feng G, Augustine GJ, Schwartz-Bloom RD. The chloride transporter Na⁺-K⁺-Cl⁻ cotransporter isoform-1 contributes to intracellular chloride increases after in vitro ischemia. *J Neurosci*. 2006; 26:1396–1406. doi: [10.1523/JNEUROSCI.1421-05.2006](https://doi.org/10.1523/JNEUROSCI.1421-05.2006) PMID: [16452663](https://pubmed.ncbi.nlm.nih.gov/16452663/)
24. Pizzarelli R, Cherubini E. Alterations of GABAergic signaling in autism spectrum disorders. *Neural Plast*. 2011; 2011:e297153. doi: [10.1155/2011/297153](https://doi.org/10.1155/2011/297153) PMID: [21766041](https://pubmed.ncbi.nlm.nih.gov/21766041/)
25. Deidda G, Bozarth IF, Cancedda L. Modulation of GABAergic transmission in development and neurodevelopmental disorders: investigating physiology and pathology to gain therapeutic perspectives. *Front Cell Neurosci*. 2014; 8:119. doi: [10.3389/fncel.2014.00119](https://doi.org/10.3389/fncel.2014.00119) PMID: [24904277](https://pubmed.ncbi.nlm.nih.gov/24904277/)
26. Inoue K, Ono H, Abe-Yoshizumi R, Yoshizawa S, Ito H, Kogure K, et al. A light-driven sodium ion pump in marine bacteria. *Nat Commun*. 2013; 4:1678. doi: [10.1038/ncomms2689](https://doi.org/10.1038/ncomms2689) PMID: [23575682](https://pubmed.ncbi.nlm.nih.gov/23575682/)
27. Kato HE, Inoue K, Abe-Yoshizumi R, Kato Y, Ono H, Konno M, et al. Structural basis for Na⁺ transport mechanism by a light-driven Na⁺ pump. *Nature*. 2015; 521:48–53. doi: [10.1038/nature14322](https://doi.org/10.1038/nature14322) PMID: [25849775](https://pubmed.ncbi.nlm.nih.gov/25849775/)
28. Kandori H. Ion-pumping microbial rhodopsins. *Front Mol Biosci*. 2015; 2:52. doi: [10.3389/fmolb.2015.00052](https://doi.org/10.3389/fmolb.2015.00052) PMID: [26442282](https://pubmed.ncbi.nlm.nih.gov/26442282/)
29. Gradinaru V, Zhang F, Ramakrishnan C, Mattis J, Prakash R, Diester I, et al. Molecular and cellular approaches for diversifying and extending optogenetics. *Cell*. 2010; 141:154–165. doi: [10.1016/j.cell.2010.02.037](https://doi.org/10.1016/j.cell.2010.02.037) PMID: [20303157](https://pubmed.ncbi.nlm.nih.gov/20303157/)
30. Hososhima S, Sakai S, Ishizuka T, Yawo H. Kinetic evaluation of photosensitivity in bi-stable variants of chimeric channelrhodopsins. *PLoS ONE*. 2015; 10:e0119558. doi: [10.1371/journal.pone.0119558](https://doi.org/10.1371/journal.pone.0119558) PMID: [25789474](https://pubmed.ncbi.nlm.nih.gov/25789474/)
31. Wood JN, Bevan SJ, Coote PR, Dunn PM, Harmar A, Hogan P, et al. Novel cell lines display properties of nociceptive sensory neurons. *Proc Roy Soc B Biol Sci*. 1990; 241:187–194. doi: [10.1098/rspb.1990.0084](https://doi.org/10.1098/rspb.1990.0084) PMID: [1979443](https://pubmed.ncbi.nlm.nih.gov/1979443/)
32. Sugiyama Y, Wang H, Hikima T, Sato M, Kuroda J, Takahashi T, et al. Photocurrent attenuation by a single polar-to-nonpolar point mutation of channelrhodopsin-2. *Photochem Photobiol Sci*. 2009; 8:328–336. doi: [10.1039/b815762f](https://doi.org/10.1039/b815762f) PMID: [19255673](https://pubmed.ncbi.nlm.nih.gov/19255673/)
33. Bertsova YV, Bogachev AV, Skulachev VP. Proteorhodopsin from *Dokdonia* sp. PRO95 is a light-driven Na⁺-pump. *Biochemistry (Mosc)*. 2015; 80:449–454. doi: [10.1134/S0006297915040082](https://doi.org/10.1134/S0006297915040082) PMID: [25869362](https://pubmed.ncbi.nlm.nih.gov/25869362/)
34. Schleich JP, Sanders CR. The safety dance: biophysics of membrane protein folding and misfolding in a cellular context. *Q Rev Biophys*. 2015; 48:1–34. doi: [10.1017/S0033583514000110](https://doi.org/10.1017/S0033583514000110) PMID: [25420508](https://pubmed.ncbi.nlm.nih.gov/25420508/)
35. Kim I, Xu W, Reed JC. Cell death and endoplasmic reticulum stress: disease relevance and therapeutic opportunities. *Nat Rev Drug Discov*. 2008; 7:1013–1030. doi: [10.1038/nrd2755](https://doi.org/10.1038/nrd2755) PMID: [19043451](https://pubmed.ncbi.nlm.nih.gov/19043451/)
36. Walter P, Ron D. The unfolded protein response: from stress pathway to homeostatic regulation. *Science*. 2011; 334:1081–1086. doi: [10.1126/science.1209038](https://doi.org/10.1126/science.1209038) PMID: [22116877](https://pubmed.ncbi.nlm.nih.gov/22116877/)

37. Wang H, Sugiyama Y, Hikima T, Sugano E, Tomita H, Takahashi T, et al. Molecular determinants differentiating photocurrent properties of two channelrhodopsins from *Chlamydomonas*. *J Biol Chem*. 2009; 284:5685–5696. doi: [10.1074/jbc.M807632200](https://doi.org/10.1074/jbc.M807632200) PMID: [19103605](https://pubmed.ncbi.nlm.nih.gov/19103605/)
38. Yizhar O, Fenno LE, Prigge M, Schneider F, Davidson TJ, O’Shea DJ, et al. Neocortical excitation/inhibition balance in information processing and social dysfunction. *Nature*. 2011; 477:171–178. doi: [10.1038/nature10360](https://doi.org/10.1038/nature10360) PMID: [21796121](https://pubmed.ncbi.nlm.nih.gov/21796121/)
39. Watanabe S, Ishizuka T, Hososhima S, Zamani A, Hoque MR, Yawo H. The regulatory mechanism of ion permeation through a channelrhodopsin derived from *Mesostigma viride* (MvChR1). *Photochem Photobiol Sci*. 2016; 15:365–374. doi: [10.1039/c5pp00290g](https://doi.org/10.1039/c5pp00290g) PMID: [26853505](https://pubmed.ncbi.nlm.nih.gov/26853505/)
40. Arrenberg AB, Del Bene F, Baier H. Optical control of zebrafish behavior with halorhodopsin. *Proc Natl Acad Sci USA*. 2009; 106:17968–17973. doi: [10.1073/pnas.0906252106](https://doi.org/10.1073/pnas.0906252106) PMID: [19805086](https://pubmed.ncbi.nlm.nih.gov/19805086/)
41. Zhang Y, Ivanova E, Bi A, Pan ZH. Ectopic expression of multiple microbial rhodopsins restores ON and OFF light responses in retinas with photoreceptor degeneration. *J Neurosci*. 2009; 29:9186–9196. doi: [10.1523/JNEUROSCI.0184-09.2009](https://doi.org/10.1523/JNEUROSCI.0184-09.2009) PMID: [19625509](https://pubmed.ncbi.nlm.nih.gov/19625509/)
42. Inada K, Kohsaka H, Takasu E, Matsunaga T, Nose A. Optical dissection of neural circuits responsible for *Drosophila* larval locomotion with halorhodopsin. *PLoS ONE*. 2011; 6:e29019. doi: [10.1371/journal.pone.0029019](https://doi.org/10.1371/journal.pone.0029019) PMID: [22216159](https://pubmed.ncbi.nlm.nih.gov/22216159/)
43. Ben-Ari Y, Cherubini E, Corradetti R, Gaiarsa JL. Giant synaptic potentials in immature rat CA3 hippocampal neurones. *J Physiol*. 1989; 416:303–325. doi: [10.1113/jphysiol.1989.sp017762](https://doi.org/10.1113/jphysiol.1989.sp017762) PMID: [2575165](https://pubmed.ncbi.nlm.nih.gov/2575165/)
44. Ueno T, Okabe A, Akaike N, Fukuda A, Nabekura J. Diversity of neuron-specific K⁺-Cl⁻ cotransporter expression and inhibitory postsynaptic potential depression in rat motoneurons. *J Biol Chem*. 2002; 277:4945–4950. doi: [10.1074/jbc.M109439200](https://doi.org/10.1074/jbc.M109439200) PMID: [11733521](https://pubmed.ncbi.nlm.nih.gov/11733521/)
45. Raimondo JV, Kay L, Ellender TJ, Akerman CJ. Optogenetic silencing strategies differ in their effects on inhibitory synaptic transmission. *Nat Neurosci*. 2012; 15:1102–1104. doi: [10.1038/nn.3143](https://doi.org/10.1038/nn.3143) PMID: [22729174](https://pubmed.ncbi.nlm.nih.gov/22729174/)
46. Li T, Yang Y, Canessa CM. A method for activation of endogenous acid-sensing ion channel 1a (ASIC1a) in the nervous system with high spatial and temporal precision. *J Biol Chem*. 2014; 289:15441–15448. doi: [10.1074/jbc.M114.550012](https://doi.org/10.1074/jbc.M114.550012) PMID: [24727474](https://pubmed.ncbi.nlm.nih.gov/24727474/)
47. Mahn M, Prigge M, Ron S, Levy R, Yizhar O. Biophysical constraints of optogenetic inhibition at presynaptic terminals. *Nat Neurosci*. 2016; 19:554–556. doi: [10.1038/nn.4266](https://doi.org/10.1038/nn.4266) PMID: [26950004](https://pubmed.ncbi.nlm.nih.gov/26950004/)
48. Kato Y, Inoue K, Kandori H. Kinetic analysis of H⁺-Na⁺ selectivity in a light-driven Na⁺-pumping rhodopsin. *J Phys Chem Lett*. 2015; 6:5111–5115. doi: [10.1021/acs.jpclett.5b02371](https://doi.org/10.1021/acs.jpclett.5b02371) PMID: [26673197](https://pubmed.ncbi.nlm.nih.gov/26673197/)